Covalency and ionicity do not oppose each other – Relationship between Si-O bond character and basicity of siloxanes*

Malte Fugel[a], Maxie F. Hesse[a], Rumpa Pal[a], Jens Beckmann[a], Dylan Jayatilaka[b], Michael J. Turner[b], Amir Karton[b], Patrick Bultinck[c], Graham S. Chandler[b], and Simon Grabowsky[a,*]

[a]University of Bremen, Department 2 - Chemistry/Biology, Institute of Inorganic Chemistry and Crystallography, Leobener Str. 3 and 7, 28359 Bremen, Germany

[b]University of Western Australia, School of Molecular Sciences, 35 Stirling Highway, Perth WA 6009, Australia

[c]Ghent University, Department of Chemistry, Krijgslaan 281 (S3), 9000 Gent, Belgium

Keywords: bonding analysis, quantum chemistry, siloxanes, basicity, covalency, ionicity

Abstract

Covalency and ionicity are orthogonal rather than antipodal concepts. We demonstrate for the case of siloxane systems ($-(R_2Si-O)_n$) that both covalency and ionicity of the Si-O bonds impact on the basicity of the Si-O-Si linkage. The relationship between the siloxane basicity and the Si-O bond character has been under debate since previous studies have presented conflicting explanations. It has been shown with natural-bond-orbital methods that increased hyperconjugative interactions of LP(O)$\rightarrow \sigma^*$(Si-R) type, i.e. increased orbital overlap and hence covalency, are responsible for the low siloxane basicity at large Si−O−Si angles. On

*Dedicated to Prof. Gerald V. Gibbs on the occasion of his 90th birthday.

the other hand, increased ionicity towards larger Si−O−Si angles has been revealed with real-space bonding indicators. To resolve this ostensible contradiction, we perform a complementary bonding analysis that combines orbital-space, real-space and bond-index considerations. We analyze the isolated disiloxane molecule $H_3SiOSiH_3$ with varying Si−O−Si angles, and n-membered cyclic siloxane systems $Si_2H_4O(CH_2)_{n\text{-}3}$. All methods from quite different realms show that both covalent and ionic interactions increase simultaneously towards larger Si−O−Si angles. In addition, we present highly accurate absolute hydrogen bond interaction energies of the investigated siloxane molecules with water and silanol as donors. It is found that intermolecular hydrogen bonding is significant at small Si−O−Si angles and weakens as the Si−O−Si angle increases until no stable hydrogen bond complexes are obtained beyond $\phi_{SiOSi} = 168^\circ$, angles typically displayed by minerals or polymers. The maximum hydrogen bond interaction energy, which is obtained at an angle of 105°, is 11.05 kJ·mol^{-1} for the siloxane-water complex and 18.40 kJ·mol^{-1} for the siloxane-silanol complex.

1 Introduction

The siloxane linkage Si−O−Si is the most common functional group in the earth's crust, where Si and O are the two most abundant elements. [1, 2] Polysiloxanes (silicones $-(R_2Si{-}O)_n-$) are indispensable in a wide variety of products used in industry and our everyday lives, e.g. supports for heterogeneous catalysts, cosmetics and coating materials. [3] The oxygen atom linking the siloxane units exhibits low Lewis basicity which results in hydrophobic material properties, whereas the analogous oxygen atom in organic ethers ($R_3C{-}O{-}CR_3$) is considerably more basic. [4] The Si−O−Si angle in most siloxane compounds is between 140° and 180°, [5–7] which is far higher than the tetrahedral angle of ≈ 110° adopted by ethers. [8] In previous studies, it has been shown that decreasing the Si−O−Si angle leads to a significant increase in the basicity of siloxanes. [4, 9–12] The Si−O−Si angle shows a high dynamic flexibility stemming from a low Si−O−Si bending potential. [13] Therefore, much smaller Si−O−Si angles can be imposed in strained cyclic siloxane systems. As suggested by the angle-basicity correlation, their basicity will be substantially higher in comparison to the basicity of siloxane units incorporated into chains and consequently they have different material properties. [9, 14–18] Hence, the coordination chemistry of cyclic siloxanes has been in the focus of very recent research. [19–23]

What is the cause of the low siloxane basicity and why does it depend on the Si-O-Si angle? The answer to these questions and also the nature of the Si−O bond, which are two inherently related aspects, are still under debate. The question has been addressed by West and Gibbs from 1960 on. [4, 24, 25] The case was reopened in 2009 with an experimental electron-density study of a siloxanol molecule, [9] which triggered recent theoretical investigations. [11, 12, 26–30] Still, diverging viewpoints are present and unreconciled: [31] While some authors ascribe a highly ionic character to the Si−O bond [9, 32], others state that it has a "substantial covalent character". [11, 12, 33] Gibbs *et al.* regard it as the "elusive bond". [34]

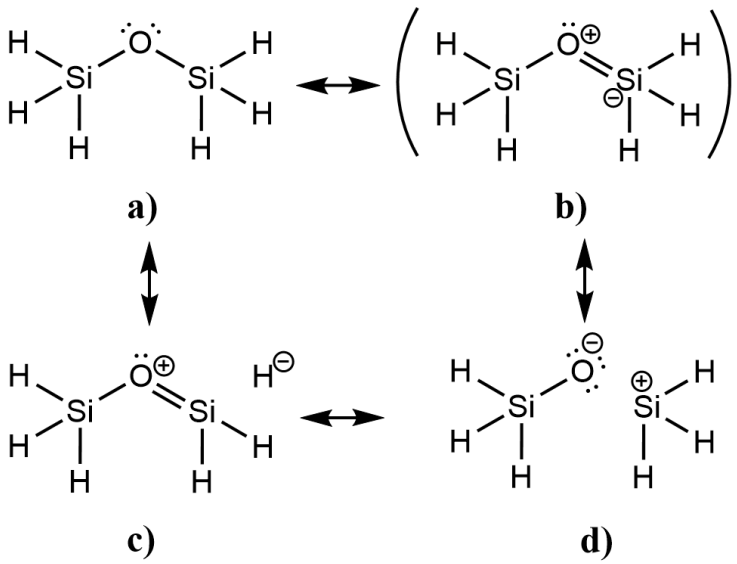

Figure 1: Possible resonance structures of disiloxane. a) Classic Lewis formula, b) obsolete hypervalent Lewis formula, c) Lewis formula resulting from hyperconjugative interactions and d) ionic Lewis formula (equivalent formulas are not depicted).

Figure 1 depicts four different Lewis structures for disiloxane $H_3Si{-}O{-}SiH_3$ which is the simplest member of the siloxane family [35, 36] and therefore a popular model system. Historically, it has been argued that the hypervalent Lewis structure **b)** is responsible for the low basicity of siloxane systems, because the electron population of the oxygen lone pairs is diminished as a consequence of n(O)→d(Si) back-bonding. [37] However, this Lewis structure is considered obsolete, because d-orbitals at the silicon atom only serve as polarization functions. [32, 38] Instead, Weinhold & West attribute the low siloxane basicity to n(O)→ σ^*(Si-R) negative hyperconjugative interactions. Lewis structure **c** is a schematic representation of this bonding model which may be

regarded as a three-center four-electron bond. [11, 12] Weinhold & West state that the siloxane basicity decreases at linear Si-O-Si angles due to the increase in intramolecular hyperconjugative interactions of LP(O)$\rightarrow \sigma^*$(Si$-$R) type, which competes with the hydrogen bonding (which is an intermolecular negative hyperconjugation of n(O)$\rightarrow \sigma^*$(H-O) type). [39] While this bonding model supports a covalent Si$-$O bond (high degree of electron sharing) that becomes more covalent with increasing Si$-$O$-$Si angle, Lewis formula **d)** suggests an ionic Si$-$O bond which is supported by studies based on various real space bonding indicators (Quantum Theory of Atoms in Molecules, electron localization functions) carried out by Grabowsky *et al.* and Gillespie & Johnson. [9,10,32] These indicators unambiguously suggest that the Si$-$O bond is highly ionic and becomes more ionic as the Si$-$O$-$Si angle increases. This study contributes towards finally resolving this ostensible contradiction. First, reliable absolute hydrogen bond interaction energies (computed from the high level, ab initio W1-F12 thermochemical protocol [40]) between the disiloxane molecule and HOX species (X = H and SiH_3) were calculated at a range of Si$-$O$-$Si angles. In addition, a variety of bonding indicators were applied to examine the bonding situation in the isolated disiloxane molecule with the Si$-$O$-$Si angle fixed between values of $\phi_{SiOSi} = 105°$ and $\phi_{SiOSi} = 180°$. The optimized geometry of the isolated disiloxane molecule is depicted in Figure 2a). In cyclic siloxane systems, smaller Si-O-Si angles and therefore a higher basicity may be imposed. Thus, the same analyses are carried out for n-membered cyclic siloxanes ($Si_2H_4O(CH_2)_{n\text{-}3}$ with n = 3, 4, 5), see Figure 2b)-d).

Since chemical bonds are not uniquely defined in quantum mechanics, there are many different bonding descriptors that attempt to extract bonding information from a molecular wavefunction. [41–43] Previous studies have shown that it is crucial to regard a variety of those bonding indicators simultaneously, because the properties obtained from them might complement and/or contradict each other, so that a reliable picture of bonding can only be obtained if all aspects are considered. [44] In this study, real-space indicators, natural bond orbital (NBO) indicators and a selection of bond indices are applied. The Quantum Theory of Atoms in Molecules (QTAIM) [45] and the analysis of the electron localizibility indicator (ELI-D) [46], both of which are applied in this study, may be classified as real-space indicators, because a real space function, which corresponds to either the electron density (in the QTAIM approach) or the ELI-D, is analyzed topologically. One

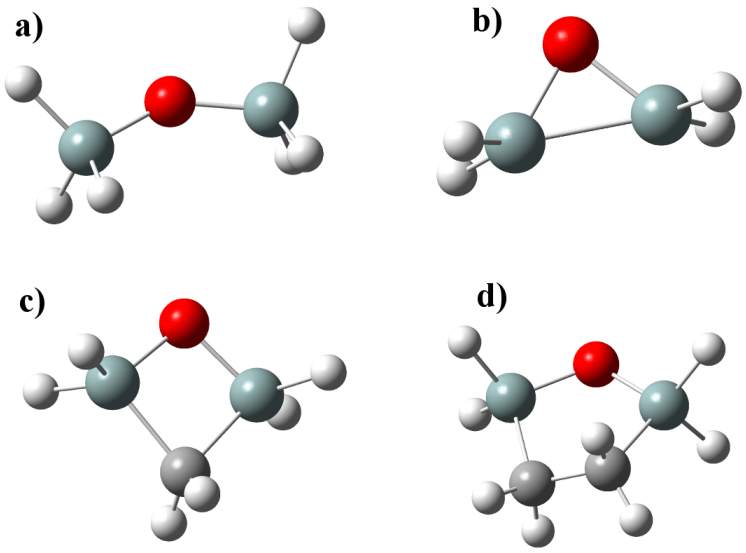

Figure 2: The structures regarded in this study with the angles from full geometry optimization: a) disiloxane (155.8°), b) 3-membered- (80.8°), c) 4-membered- (96.2°) and d) 5-membered (116.1°) siloxane rings

can look at critical points, where the gradient of the real-space function disappears ($\nabla f(\vec{r}) = 0$), and integrate properties for basins that are defined topologically by the zero-flux surface, where $\nabla f(\vec{r}) \cdot \vec{r} = 0$. In QTAIM, these basins may be related to atoms and their integration yields atomic charges (Bader charges). In the ELI-D, basins are related to the shell structure, bonds and lone pairs and, through integration of the electron density inside them, their electron populations are obtained. The source function is an extension of the QTAIM where the contribution of atomic basins to the electron density at a reference point (mostly a bond critical point) may be revealed. [47]. Natural bond orbitals (NBOs) may be associated with features of Lewis structures such as bonds and lone pairs. [39, 48] There are also non-Lewis NBOs such as valence anti-bonds or extravalent Rydberg-type NBOs which normally have a low electron population. In this study, it is of particular interest to investigate the interaction between donor (Lewis-type) and acceptor (non-Lewis-type) NBOs in the context of negative hyperconjugation in the siloxane systems (LP(O)$\rightarrow$ σ^*(Si-R)). We will also analyze the results from natural resonance theory (NRT) which attempts to approximate the true density matrix with the sum of weighted localized density matrices. [49–51] This method yields the natural bond order which is analyzed alongside another four bond indices: The NLMO/NPA bond order (from the NBO analysis) [39], the delocalization index (from the QTAIM analysis) [52], the Hirshfeld-I shared electron density index (SEDI) [53] and the Roby-

Gould bond index. [54] In Section 4, the procedure of the complementary bonding analysis is described and a theoretical background is provided for different definitions of atoms in molecules and bond indices.

2 Results and discussion

2.1 Hydrogen bond energies of siloxane···HOX complexes

Figure 3 shows the interaction energies of the two hydrogen bond complexes plotted against the Si−O−Si angle. The energies were obtained according to Equation 1, where E(siloxane) refers to the molecular energy of the fully optimized cyclic siloxane or partially optimized disiloxane molecule (with frozen Si−O−Si angle), $E(H_2O)$ refers to the energy of a fully optimized water molecule and E(siloxane···HOX) refers to the fully optimized cyclic siloxane···H_2O complex or partially optimized disiloxane···HOX complex.

$$E_{int} = E(\text{siloxane}) + E(H_2O) - E(\text{siloxane}\cdots\text{HOX}) \quad (1)$$

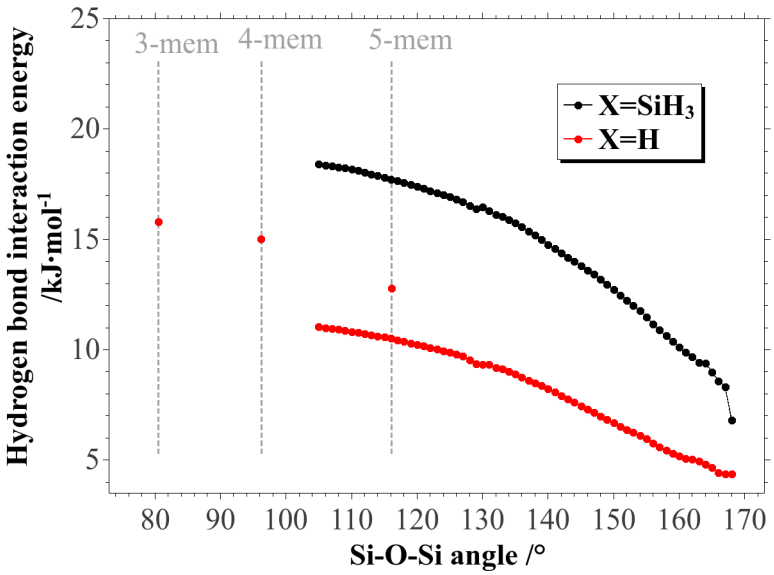

Figure 3: The hydrogen bond energies (ZPVE corrected) of disiloxane···HOX (X = H and SiH_3 and n-membered cyclic siloxane···HOH (n = 3,4,5) complexes at the W1-F12/A'VTZ level of theory

The interaction energies of both complexes decrease continuously up to an Si−O−Si angle of $\phi_{SiOSi} = 168°$, above which no convergence for the complex geometries was achieved. Conse-

quently, hydrogen bonding becomes unfeasible for angles higher than $\phi_{SiOSi} = 168°$, which is similar to previous findings. [9,10] In contrast to previous results, the absolute values of the hydrogen-bond energy are reliable and can be used as thermochemical reference properties because of the substantially higher level of theory used. It is also evident that H_3SiOH is a significantly better hydrogen bond donor than water, because the corresponding interaction energies are higher. [55] The maximum hydrogen bond interaction energy, which is obtained at an angle of 105°, is 11.05 kJ·mol^{-1} for the siloxane-water complex and 18.40 kJ·mol^{-1} for the siloxane-silanol complex. At $\phi_{SiOSi} = 156°$, which is the calculated point closest to the fully relaxed geometry of free disiloxane $H_3SiOSiH_3$ (155.8°, see Figure 2), the values drop to 5.75 kJ·mol^{-1} for the siloxane-water complex and 11.17 kJ·mol^{-1} for the siloxane-silanol complex, before they become insignificant at Si−O−Si angles larger than 168°.

Figure 3 also shows the hydrogen bond interaction energies of the n-membered (n = 3, 4, 5) cyclic siloxane···HOH complexes. As expected from the angle-basicity correlation, the interaction energies decrease with increasing Si−O−Si angle: The highest interaction energy is obtained for the 3-membered ring (15.80 kJ·mol^{-1}), an intermediate energy for the 4-membered ring (15.01 kJ·mol^{-1}), while the 5-membered ring shows the lowest interaction energy (12.78 kJ·mol^{-1}). Overall, the trend of the cyclic siloxane systems is shifted towards higher interaction energies in relation to the disiloxane···HOH complexes, i.e. hydrogen bonding is more favorable in the cyclic systems. The Si−O−Si angle is not the only factor determining the basicity of siloxanes, i.e. the substitution on the silicon also plays an important role, especially if hyperconjugative interactions of LP(O)→ σ^*(Si-R) type are regarded as the main cause of the low siloxane basicity.

2.2 Bonding analysis of the siloxane systems

NBO analysis. The NBO analysis enables us to look at the interaction between Lewis-type and non-Lewis-type NBOs, and, thus, it may reveal the negative hyperconjugation of n(O)→ σ^*(Si−R) type in a straightforward way (Figure 4) as it has previously been done by Weinhold and West for permethylated siloxanes. [11,12] In the following, the NBOs which are involved in this interaction are inspected in detail.

The NBO analysis yields two different types of oxygen lone pair NBOs. One is completely of

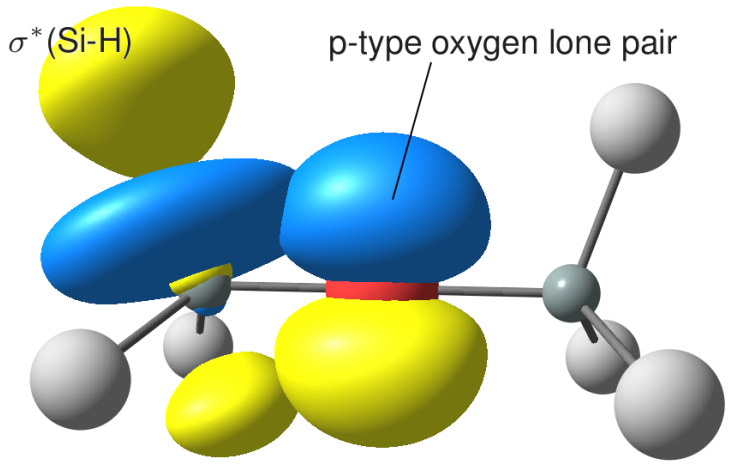

Figure 4: Hyperconjugative interaction at the linear Si−O−Si angle of the disiloxane model compound visualized as overlap of an oxygen lone-pair NBO (LP(O)) and the Si-H anti-bonding NBO. At the linear geometry, both oxygen LP(O) NBOs are identical, see Figure 5.

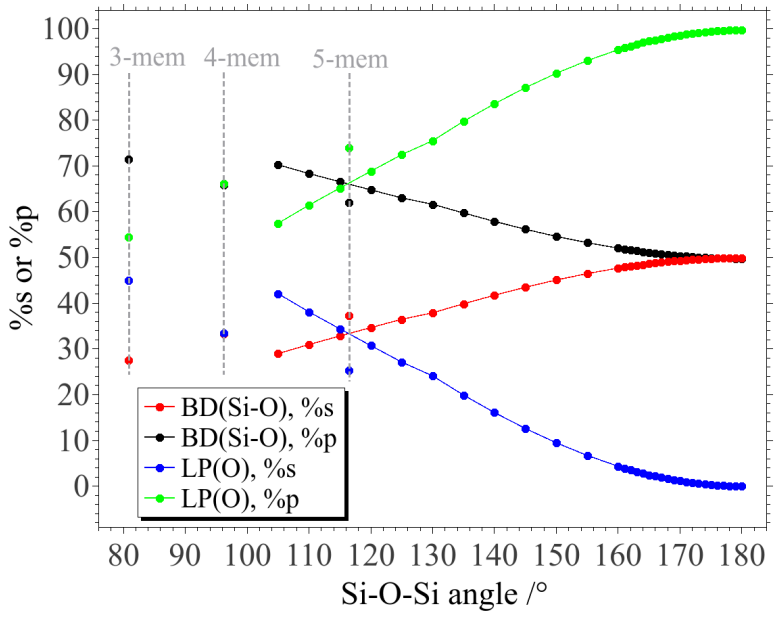

Figure 5: The hybridization in terms of percentage s- and p-character of the sp^{λ}-type oxygen lone pair NBO ($\lambda = \%p/\%s$) and the oxygen atomic hybrid orbital that is involved in the Si-O bonding NBO BD(Si-O) plotted against the Si−O−Si angle. The second LP(O) is of pure p-character and therefore not shown here.

p-character for the whole range of Si−O−Si angles, while the hybridization of the other changes from $\approx sp^{1.4}$ to completely p-character as the Si−O−Si angle becomes larger (Figure 5, green and blue). Consequently, the oxygen hybrid orbital that forms the Si−O bond must also undergo rehybridization (Figure 5, black and red). As the oxygen lone pair gains in p-character, the p-character of the oxygen bonding hybrid orbital decreases. At $\phi_{SiOSi} = 105°$ the oxygen bonding hybrid is $\approx sp^{2.4}$ which changes smoothly to sp-character as the Si−O−Si angle opens, which

is in agreement with Coulson's orthogonality theorem. [56] Since the hybridization of the two oxygen lone pairs differs, particularly at bent Si−O−Si angles, their contribution to the negative hyperconjugation is different. This may be revealed by inspecting the oxygen lone pair populations N(LP(O)), previously considered by Weinhold *et al.* [11], and delocalization energies related to the LP(O)→ σ^*(Si-H) interactions (Figure 6). If N(LP(O)) is low, it follows that the negative hyperconjugation is strong, since electron density is shifted from the oxygen lone pairs to the σ^*(Si-H) NBOs.

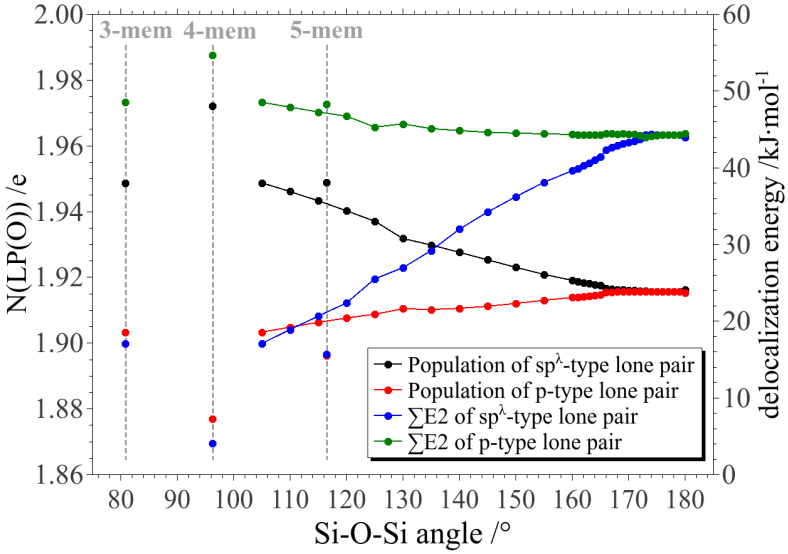

Figure 6: The oxygen lone pair populations, N(LP(O)), and the summed delocalization energies, $\sum$E2, which can be attributed to the LP(O)→ σ^*(Si-H) interactions of the siloxane systems plotted against the Si−O−Si angle

Figure 6 shows that N(LP(O)) of the sp$^\lambda$-type oxygen lone pair decreases with increasing Si−O−Si angle, i.e. its involvement in the negative hyperconjugation becomes more significant as it gains in p-character. For the p-type lone pair, the opposite trend is observed: Its electron population increases slightly. This is in agreement with the LP(O) delocalization energies. For the sp$^\lambda$-type lone pair the delocalization energy increases, which causes a higher stabilization of the molecule resulting from this interaction, while the delocalization energy of the p-type oxygen lone pair decreases slightly. At nearly linear Si−O−Si angles, the two lone pairs become indistinguishable in terms of their hybridization, their electron populations and delocalization energies. A natural bond orbital analysis of the disiloxane-water complexes shows that the hydrogen bonding is related to the hyperconjugative interaction involving the sp$^\lambda$-type oxygen lone pair (donor orbital) and one anti-bonding O−H orbital of H_2O (acceptor orbital). Consequently, the rehybridization

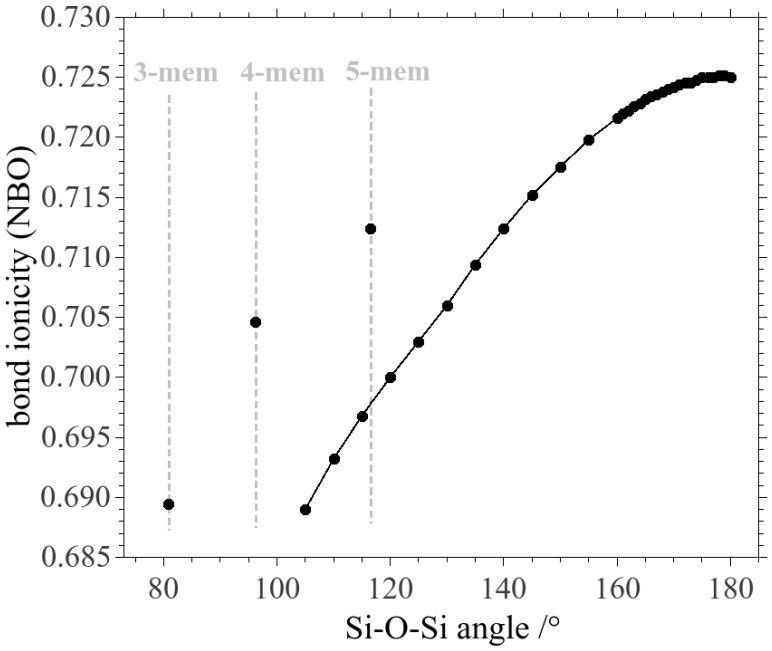

Figure 7: NBO bond ionicity parameter

of the sp^{λ}-type lone pair to completely p-character is responsible for the weakening of hydrogen bonding at higher Si−O−Si angles. In the Supporting Information the interacting orbitals are depicted alongside the respective E2 values, which are a measure of the strength of the interaction.

The results for the n-membered cyclic siloxane systems support the conclusion of the previous paragraph. For these ring systems Figure 5 shows that the sp^{λ}-type oxygen lone pair has a higher p-character and the oxygen bonding hybrids have, in turn, higher s-character than suggested by the angular trend in the disiloxane molecule. For the disiloxane molecule, an increase in p-character is indicative of the stronger intramolecular hyperconjugation and thus a lower basicity. However, in the ring systems the jump in p-character as compared with the open siloxane molecule is associated with a decrease in hyperconjugation as evidenced by increased sp^{λ} electron populations of the ring systems shown in Figure 6 and the lower delocalization energies from the LP(O) $\rightarrow$ σ^*(Si-R) delocalization, also shown in Figure 6. This decrease in hyperconjugation correlated with the increased basicity shown by the higher hydrogen bond energies of the ring system, illustrated in Figure 3, reinforces the conclusion that from the point of view of NBO analysis LP(O)$\rightarrow$ σ^*(Si-R) negative hyperconjugation is the driver of the basicity. While there is a σ^*(Si−C) acceptor bond in the 4- and 5-membered rings, there is a σ^*(Si−Si) acceptor bond in the 3-membered ring. Therefore one should not expect the 3-membered ring values to align with the 4- and 5-membered

rings.

The NBO analysis showed that there is an overall increase in hyperconjugative interactions and hence covalent contributions with increasing angle. This is in line with decreased basicity. However, the very same NBO analysis also reveals a different trend, namely an increase in ionicity with increasing Si−O−Si angle (Figure 7). Weinhold *et al.* defined the bond ionicity in terms of the polarization coefficients of the silicon and oxygen hybrid atomic orbitals which form the Si-O NBO and already applied it to the disiloxane molecules at varying Si-O-Si angle, [11, 39] shown in Figure 7 for our calculations.

Bond critical point properties. The electron density at the Si−O bond critical points (ρ_{bcp}(Si-O)) and the Si−O bond length r(Si-O) are plotted against the Si−O−Si angle in Figure 8. The increase

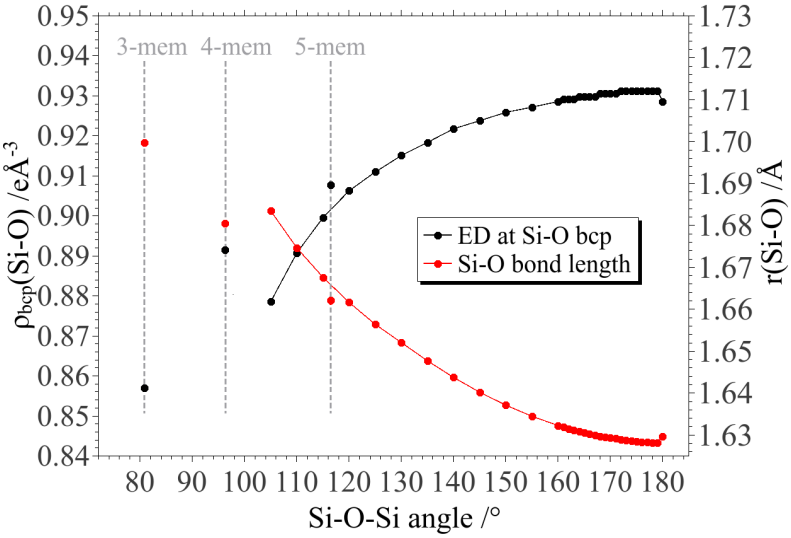

Figure 8: The electron density at the Si−O bond critical point, ρ_{bcp}(Si-O), and the silicon-oxygen bond length, r(Si-O), of the disiloxane and n-membered cyclic siloxane systems plotted against the Si−O−Si angle

in ρ_{bcp}(Si-O) and the simultaneous decrease in r(Si-O) in the disiloxane molecules may be related to an increase in the partial Si-O double bond character, as shown in Lewis structure **c)** in Figure 1, which is a representation of the negative hyperconjugative interactions. For the ring system, the same trend is observed for ρ_{bcp}(Si-O), although shifted to higher values which implies an even higher partial Si-O double bond character, and, thus, overall stronger hyperconjugative interactions. At first glance, this is contradictory to the higher hydrogen bond energies of the ring systems because stronger hyperconjugative interactions should lead to a lower siloxane basicity. However, in the preceding section, it was shown that the low siloxane basicity is caused by intramolecular

hyperconjugation that the sp^{λ}-type oxygen lone pair is involved in, but when regarding ρ_{bcp}(Si-O) we see the effect from both the sp^{λ}- and p-type lone pairs.

Figure 9 shows the Laplacian (the second derivative of the electron density) at the Si-O bond critical point $\nabla^2\rho_{bcp}$(Si-O) plotted against the Si−O−Si angle. The Laplacian is highly positive for

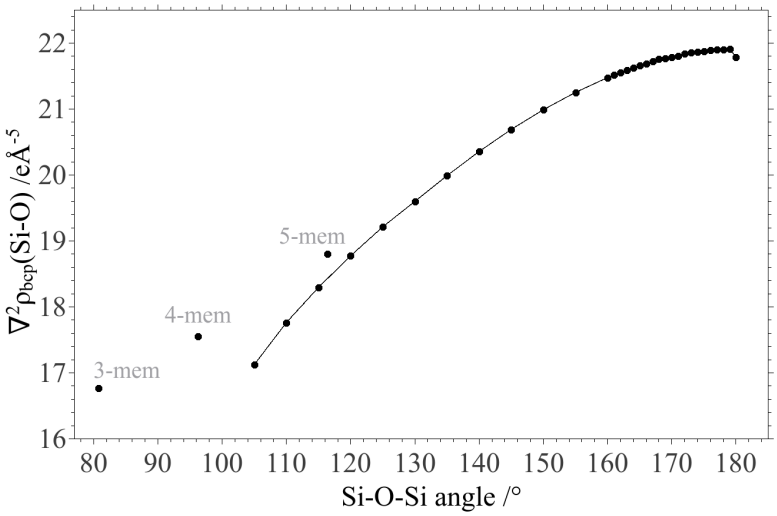

Figure 9: The Laplacian of the electron density at the Si−O bond critical point, $\nabla^2\rho_{bcp}$(Si-O), of the disiloxane and n-membered cyclic siloxane systems plotted against the Si−O−Si angle

all Si−O−Si angles which is an indication for a highly polarized Si−O bond [44, 45]. The increase in $\nabla^2\rho_{bcp}$(Si-O) indicates that the Si-O bond becomes even more polarized as the Si−O−Si angle becomes more linear. Interestingly, two properties at the bond critical point of the electron density give two opposing characterizations of the Si-O bond. While ρ_{bcp}(Si-O) suggests an increase in covalency, $\nabla^2\rho_{bcp}$(Si-O) implies an increase in ionicity. In the Supporting Information, we show the total energy density at the Si−O bond critical point plotted against the Si−O−Si angle. This plot also implies the Si−O bond to become increasingly ionic.

Analysis of the source function. The source function is analyzed with respect to the contribution of the QTAIM oxygen basin to the electron density at the Si−H bond critical points. This is of particular interest because this contribution may be related to the hyperconjugative interactions of LP(O)→ σ^*(Si-H) type. Figure 10 depicts the sum of the percentage contributions of the oxygen basin to the electron density at the bond critical points of all Si-H bonds of a SiH_3 group plotted against the Si−O−Si angle.

The contribution of the oxygen basin to the electron density at the Si−H bond critical points

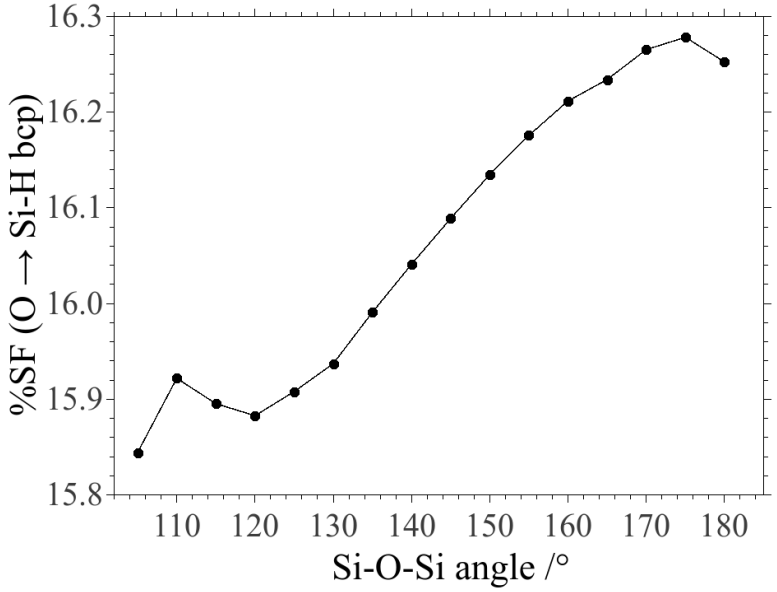

Figure 10: Source function given as the sum of the percentage contributions of the oxygen basin to the electron density at the bond critical points of all Si-H bonds of a SiH_3 group

is exceptionally high for the whole range of Si−O−Si angles, [47] which is a measure of negative hyperconjugation. The remaining contributions come almost exclusively from the neighboring silicon and hydrogen atoms. After no clear trend is recognizable for the first three data points, the contribution of the oxygen atom increases steadily with increase in the Si−O−Si angle which correlates with an increase in negative hyperconjugation.

Analysis of the ELI-D. The electron localizibility indicator ELI-D is a measure of electron localization – electrons are less perturbed in regions where values of the ELI-D are high. The analysis yields different types of basins that are defined by the topology of the ELI-D: there are core basins, monosynaptic basins (in contact with one core basin) which may be related to lone pairs and disynaptic basins (in contact with two core basins) which may be related to bonds. These ELI-D basins are different to those from QTAIM associated with the electron density, and they also have no direct relation to the bonds and lone pairs from the NBO analysis, which correspond to the localized orbital picture rather than to the real space picture. This is because of the completely different techniques used for dividing space.

Figure 11 shows the electron populations of the valence basins, i.e. the oxygen lone pair and Si−O bond basins, plotted against the Si−O−Si angle. The total number of electrons inside the valence basins of the disiloxane molecules is approximately the same for all Si−O−Si angles.

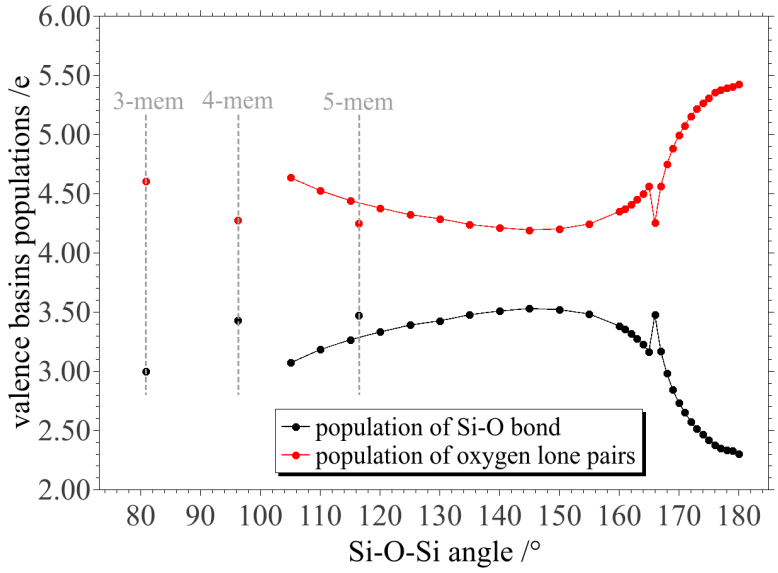

Figure 11: The ELI-D oxygen lone pair and Si−O bond populations of the disiloxane and n-membered cyclic siloxane systems plotted against the Si−O−Si angle

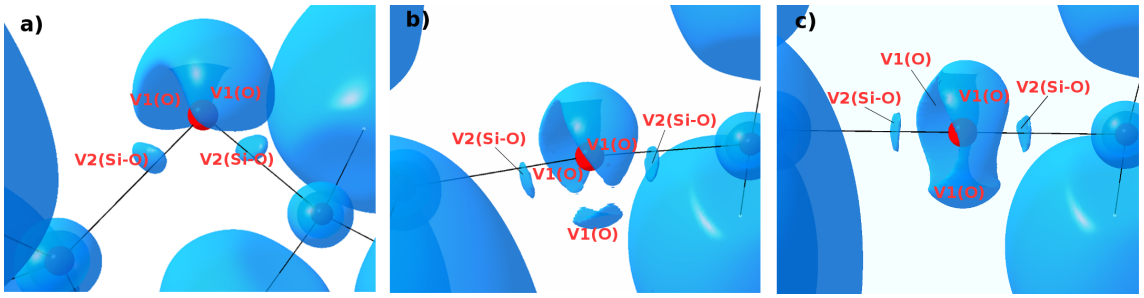

Figure 12: ELI-D iso-surfaces showing the oxygen lone pair (V1(O)) and Si−O bond (V2(Si-O)) localization domains of the disiloxane molecules at Si−O−Si angles of a) $\phi_{SiOSi} = 105°$ (ELI-D$_{iso}$ = 1.53), b) $\phi_{SiOSi} = 170°$ (ELI-D$_{iso}$ = 1.52) and c) $\phi_{SiOSi} = 180°$ (ELI-D$_{iso}$ = 1.52)

Starting from $\phi_{SiOSi} = 105°$ up to $\phi_{SiOSi} = 145°$, the lone pair population decreases while the bond population increases. The initial trend is then reversed until a sudden jump appears at $\phi_{SiOSi} = 166°$ which is in close proximity to the angle after which hydrogen bonding becomes unfeasible. After that jump the lone pair population increases steeply. This is accompanied by a steep decrease in the Si−O bond population. The total number of electrons inside the oxygen lone pairs is lowest in the region where hydrogen bonding is feasible. This shows that the total charge around the oxygen atom is not decisive for its basicity, but that this charge must both be concentrated and localized in a suitable way to allow the oxygen atom to act as a base.

The iso-surfaces of the ELI-D may be visually analyzed to understand the way charge is localized around the oxygen atom. In Figure 12, three iso-surfaces at different Si−O−Si angles are depicted. At $\phi_{\mathrm{Si-O-Si}} = 105°$ (Figure 12a), there is a cashew-shaped lone pair domain located at the

oxygen atom. The shape remains that way throughout all the angles that allow stable hydrogen bond complexes. Here, electrons are localized in a region where a proton would approach in an electrophilic attack. Starting from $\phi_{\mathrm{Si-O-Si}} = 166°$, which is the angle where the ELI-D valence population shows a jump and close to the angle where hydrogen bonding ceases, an additional attractor located underneath the oxygen atom opposite to the cashew-like lone pair appears (Figure 12b). The localization of electrons at this position may be related to the sp^{λ}-type lone pair NBO which is almost of complete p-character at this angle (see Figure 5). The s-character of this lone pair NBO is higher at lower Si−O−Si angles, which explains why the appearance of this attractor occurs only at high angles when the p-character far outweighs the s-character. As the angle opens even further, the three oxygen lone pair domains become increasingly indistinguishable until they are identical at $\phi_{\mathrm{Si-O-Si}} = 180°$. Figure 12c shows that the three equivalent lone pair domains form a ring at this angle. The formation of a ring at angles $\phi_{Si-O-Si} \geq 168°$ and a high electron population of $N \gg 4$ is characteristic for an oxygen atom that is involved in an ionic bond [44], here corresponding to resonance form d) in Figure 1.

For the cyclic siloxane systems, the lone pair populations are lower and Si−O bond populations higher compared to the trend of the disiloxane molecules. Here, we cannot make the same argument we made in the NBO analysis: A lower ELI-D lone pair basin population does not result in a lower basicity.

Atomic charges. Since there are many different approaches to define an atom inside a molecule as discussed in the Theoretical methods part, there is no unambiguous definition for an atomic charge. The QTAIM and NBO analysis yield the Bader and NPA charges, respectively. Another approach to obtain atomic charges are the Hirshfeld-I charges which are retrieved by iteratively applying Hirshfeld's stockholder partitioning scheme. [57] It is always beneficial to regard a variety of different approaches, because the magnitude of these charges is conflicting, e.g. the Bader charges are known to suggest a substantially more ionic picture compared to the other charges. [58]

Figure 13 shows the Bader, NPA and Hirshfeld-I charges plotted against the Si−O−Si angle. The Si charges of the n-membered rings are not shown here since the Si atoms have different bonding partners. Despite the different methods used in obtaining these charges, they show the same trend as the angle increases. The charge of the silicon atom becomes more positive while the

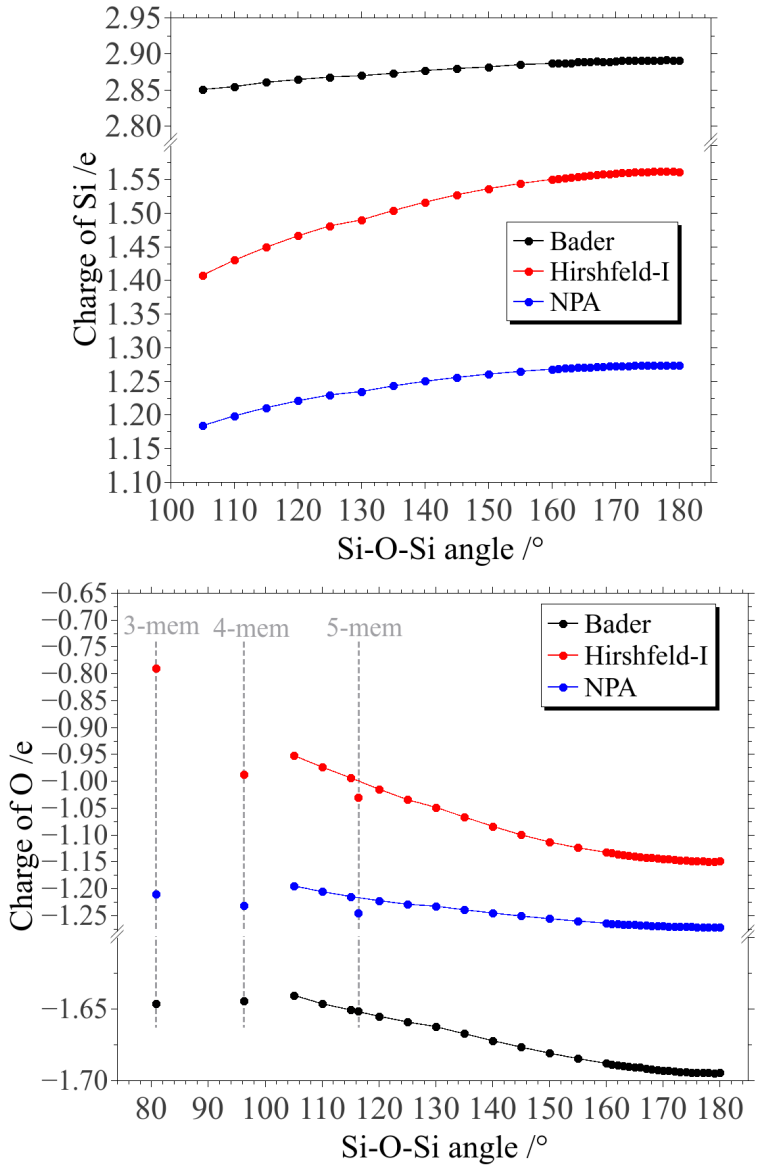

Figure 13: The Bader, Hirshfeld-I and NPA charges of the silicon (top) and oxygen (bottom) atoms plotted against the Si−O−Si angle

charge of the oxygen becomes more negative. Thus, the charge separation between the silicon and oxygen atom increases – the Si−O bond becomes more ionic, which is confirmed by the Laplacian values at the Si−O bond critical point. This would suggest that Lewis formula **1d** in Figure 1 becomes more significant at increasing Si−O−Si angle which, at first glance, is contradictory to an increase in hyperconjugative interactions. If the increase in ionicity is related to increased electronegativity of the oxygen atom, then electrons should also be withdrawn from the hydrogen atoms of the SiH_3 group. However, Figure 14 shows that the total charge of the hydrogens becomes more negative with increasing Si−O−Si angle. This increase can be related to the increase in

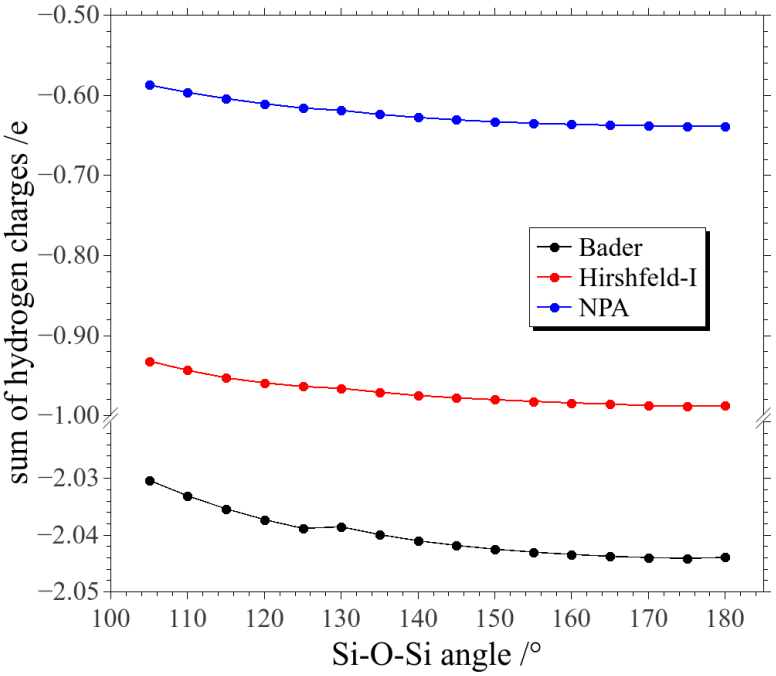

Figure 14: The sum of the Bader, Hirshfeld-I and NPA charges of the three hydrogen atoms of one SiH_3 group plotted against the Si−O−Si angle

hyperconjugative interactions because they result in a shift in electron density into the σ^*(Si−H) bonds thus increasing the charge of the hydrogen atoms and corresponding to the resonance form **1c** in Figure 1.

Bond indices. In the following, five different types of bond indices – the Hirshfeld-I SEDI, the Roby-Gould bond index, Bader's delocalization index (DI), the NLMO/NPA bond order and the natural bond order based on a natural resonance theory (NRT) analysis – will be analyzed. Figure 15 shows these bond indices plotted against the Si−O−Si bond angle. All values of the Hirshfeld-I SEDI are above a value of one, while the DI, which is also a SEDI, is substantially lower than one. The difference between the Hirshfeld-I SEDI and the DI is the definition of the atom applied in each of these approaches. The charges of the respective atoms (the Hirshfeld-I and Bader charges) have been discussed in the preceding section, where the Bader charges have been found to imply a substantial charge separation between the silicon and oxygen atoms, i.e. highly ionic Si−O bonds. The DI shows substantially lower values compared to the Hirshfeld-I SEDI, which directly follows from the different nature of Bader and Hirshfeld-I charges. A highly positive Bader charge of the silicon atom comes with a small atomic volume, and, thus, the number of electron pairs exchanged between the silicon and oxygen atom is lower, because they are contained in the larger

oxygen atom. The Hirshfeld-I silicon atom is larger and the oxygen atom is smaller compared to the corresponding Bader atoms. Consequently, more electron pairs are exchanged between these atoms, which results in larger bond indices.

The NLMO/NPA bond order is defined as the overlap of natural localized molecular orbitals (NLMO) and atomic populations obtained from the natural population analyis (NPA); therefore, it is derived in a substantially different way compared to the other bond indices. Its values are even lower than the DI, and, thus, suggest an even more ionic Si−O bond. On the other hand, the natural bond order is similar to the Hirshfeld I SEDI, whereas the Roby-Gould index is higher.

The Roby-Gould bond index, Hirshfeld-I SEDI and the natural bond order increase with increasing Si−O−Si angle, suggesting the partial Si−O double bond character to gain in significance. The DI, on the other hand, decreases with increasing Si−O−Si angle, which may be attributed to the fact that the Si−O bond becomes even more ionic with increasing Si−O−Si angle thus reducing the number of exchanged electron pairs. Just as the DI, the NLMO/NPA bond order decreases with increasing Si−O−Si angle. It is interesting that out of the five bond orders considered in this study, three support an increase in partial Si−O double bond character with increasing Si−O−Si angle, while the other two support a highly ionic Si−O bond description. Consequently, the definition of the atom greatly influences the picture of the bonding situation provided to us and makes meaningful chemical interpretation very difficult.

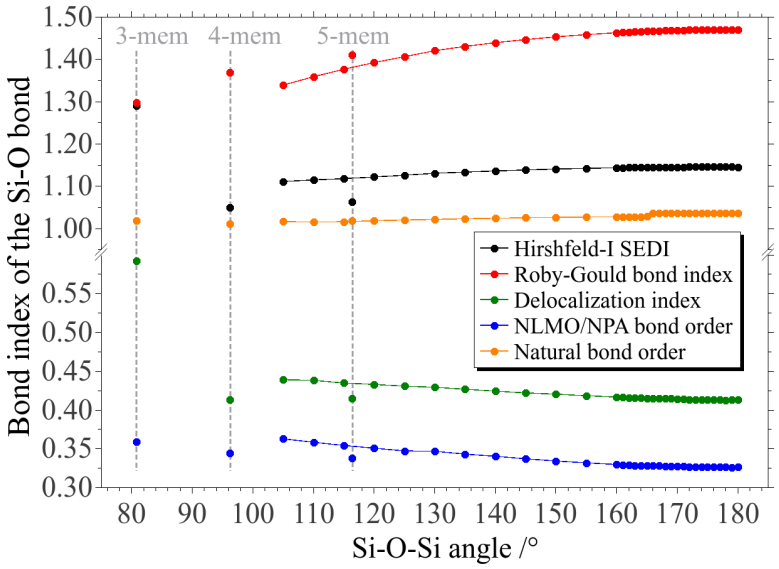

Figure 15: Five different bond indices (Hirshfeld-I SEDI, Roby-Gould bond index, delocalization index, NLMO/NPA bond order and natural bond order) of the disiloxane and n-membered cyclic siloxane systems plotted against the Si−O−Si angle.

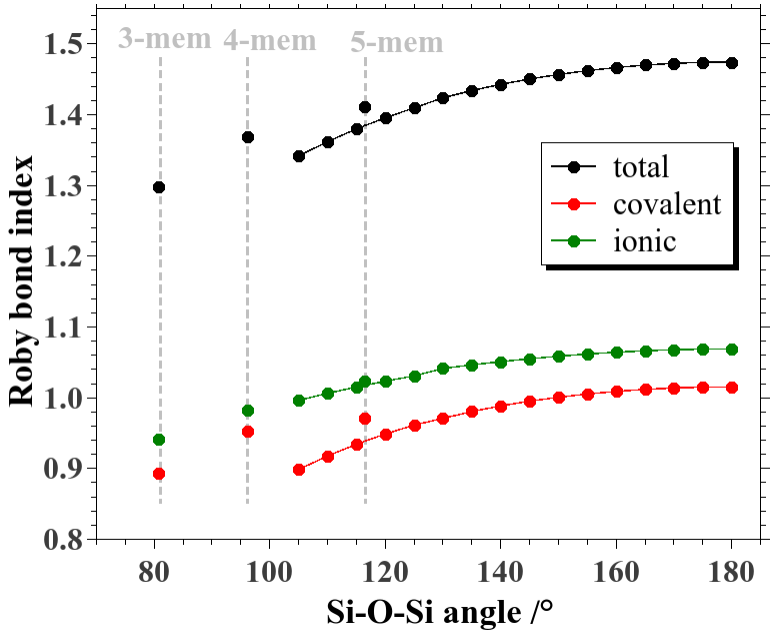

Figure 16: Covalent, ionic and total Roby-Gould bond indices

The Roby-Gould bond index has a total, a covalent and an ionic part as derived in the Theoretical methods part. This allows comparison of the behaviour of covalent and ionic contributions to the bonding within the same definition of an atom, avoiding the problems discussed in the previous paragraph. Figure 16 clearly shows that ionic and covalent contributions have about the same importance for the overall description of the Si-O bond character, and that both increase simultaneously with increasing angle. Hence, covalency and ionicity support and complement each other in increasing the bond order, and consequently bond strength, of the Si-O bond.

The cyclic siloxane systems agree well with the trend of the Roby-Gould bond index. The Hirshfeld-I SEDI, however, implies that the nature of the Si−O bond is different in the ring systems (Figure 15). For the 3-membered ring, the Hirshfeld-I SEDI is substantially higher, while it is slightly lower for the 4- and 5-membered rings which may be related to the weaker intramolecular hyperconjugative interactions. The trend of the NLMO/NPA bond order shifts to lower values than suggested by the disiloxane molecules. While this shift is also true for the 5- and 4-membered rings in the delocalization index, the 3-membered ring shows an anomalously high delocalization index. These shifts may be attributed to the higher ionic nature of the Si−O bond in the cyclic siloxane systems. This does, however, not apply to the delocalization index of the 3-membered ring.

3 Conclusion

In contrast to all previous studies on siloxanes, a wide range of bonding indicators has been used in the present study in the sense of a *complementary bonding analysis* to understand the nature of the Si−O bond and the reason for the strong dependence of the siloxane basicity on the Si−O−Si angle. Various bond indicators present different pictures of bonding and relating these to each other is not simple. Especially when sigificantly different definitions of an atom are used, charges and bond indices differ so significantly in terms of absolute values and in terms of trends in dependence of the Si−O−Si angle that chemical interpretation becomes a gamble. If one relies on a single one of these bonding descriptors or methods for chemical interpretation, as we and others have done in the past in the field of siloxanes, incomplete and insufficient pictures arise.

We have found in this study that in four different methods a simultaneous covalent and ionic description of the Si-O bond and a simultaneous increase in both covalency and ionicity with increasing Si−O−Si angle is present. As this is inherent to the same method, all inconsistencies of definitions discussed in the previous paragraph are irrelevant. i) In NBO, increased negative hyperconjugation with increasing Si−O−Si angle is accompanied by an increase in the bond ionicity which is defined through the same weighting coefficients that determine the NBOs which are engaged in the negative hyperconjugative interactions. ii) In QTAIM, electron density accumulates in the Si-O bond with increasing Si−O−Si angle, and the Laplacian indicates increased closed-shell interactions simultaneously. iii) The Si – O charge separation increases with increasing Si−O−Si angle revealing an increase in ionicity, while the hydrogen atoms become more negative which represents increased negative hyperconjugation. These trends are the same in QTAIM, NPA and Hirshfeld-I charges. iv) The total Roby-Gould bond index is made up of a covalent and an ionic bond index, both of which increase simultaneously with increasing Si−O−Si angle. Their absolute values are also very similar indicating that ionicity and covalency have about the same importance for the Si-O bond. All of the findings summarized in this paragraph clearly show that covalency and ionicity do not oppose each other, but are two complementing properties of the Si-O bond.

This study is an example of the fact that a single Lewis formula can never fully reflect the bonding situation in a molecule especially when lone pair or bond delocalizations are of great significance. For the siloxane molecules, Lewis formula **c)** in Figure 1 indicates negative hypercon-

jugation, i.e. covalency, whereas Lewis formula **d)** represents an ionic Si−O bond. Both resonance forms have about the same importance for the bonding situation, and both gain in importance simultaneously when the Si−O−Si angle increases. We believe that also in chemical systems other than the siloxanes, more insights into bonding situations can be obtained when the textbook notion of covalency and ionicity as antipodes is dropped.

For the chemistry of siloxanes, we plan to synthesize a systematic array of molecular compounds with different Si−O−Si angles to study the tuning of material properties based on the findings of this study. Design of materials with hydrophilic properties might be possible if a desired Si−O−Si angle can be manifested in a template ring structure. This could have implications for heterogeneous catalysis where siloxanes are used as supports. Certainly, further insights into the properties of minerals can be gained this way since Gibbs has argued for many years that "molecules [are] models for bonding in silicates". [25]

4 Methodology and theoretical background

4.1 Geometry optimizations

Geometry optimizations of the disiloxane molecule and the n-membered cyclic siloxane systems $Si_2H_4O(CH_2)_{n\text{-}3}$ were carried out at the B3LYP/A'VTZ level of theory, [59, 60] using the Gaussian 09 program suite. [61] The resulting structures were confirmed to be equilibrium structures via harmonic vibrational calculations (i.e. they have all real frequencies). In addition, a relaxed potential-energy surface scan was carried out for the disiloxane molecule between Si−O−Si angles of $\phi_{SiOSi} = 105°$ and 160° in 5° intervals and $\phi_{SiOSi} = 160°$ and 180° in 1° intervals.

4.2 Bonding analysis

NBO analyses were carried out with NBO6.0. [62] The program suite AIMall was applied for the QTAIM analysis and the calculation of the source function. [63] The computation of the ELI-D and its topological analysis were performed with DGrid-4.6 [64]. Related ELI-D isosurfaces were plotted with the program Moliso. [65] The Roby-Gould bond index was calculated using the Tonto software package. [66] Hirshfeld-I charges and SEDIs were calculated with self-written software.

4.3 Hydrogen bond interaction energies

In order to obtain reliable absolute hydrogen bond interaction energies between the siloxane and HOX species (X = H and SiH_3), calculations were carried out using the high-level ab-initio W1-F12 thermochemical protocol with the Molpro 2012.1 program suite. [67] The W1-F12 thermochemical protocol [68] and its earlier version W1 [40] are widely used for the calculation of thermochemical and kinetic properties. [69, 70]

The calculations were performed on the B3LYP/A'VTZ geometries of the fully optimized cyclic siloxanes, water and silanol molecules as well as of the partially optimized disiloxane molecules and their HOX (X = H or SiH_3) complexes from PES scans with Si-O-Si angles constrained to $\phi_{SiOSi} = 105^\circ$ to 180° in 1° intervals. Energy differences according to Eq. 1 at the W1-F12 level were calculated with and without zero-point vibrational energy (ZPVE) correction.

4.4 Theoretical background

One of the main problems in analyzing chemical bonding is that many of the ideas and concepts that are so central to chemistry, for instance identifying atoms in molecules or chemical bonds, do not emanate so simply from quantum mechanics. [71] In fact, quantum mechanics does not give a unique recipe to distinguish atoms in molecules [72] or chemical bonding and the best one can do, if one values these concepts, is to propose models or algorithms that rely on sane arguments such as variational principles or projection operators to extract atoms and bonds from the wavefunction. Still, this will not lead to a unique description. As one of the main purposes of the present study is the comparison of methods, we now introduce these methods to the level of detail required here. The NBO method is well known and has been described in detail elsewhere, [39, 48] therefore, it is not discussed further.

A key role will be played by the density operator and matrix. Denoting the wavefunction as Ψ, the density operator is given by:

$$\hat{D} = |\Psi\rangle \langle\Psi| . \tag{2}$$

Stepwise integration over all electronic coordinates except one or two electronic position coordi-

nates, leads to the first and second order reduced density operators which may be expressed in the basis of the natural orbitals (NOs) as

$$\hat{\gamma} = \sum_i |i\rangle \, \eta_i \, \langle i| \tag{3}$$

and

$$\hat{\Gamma} = \sum_{ijkl} |ij\rangle \, \Gamma_{ijkl} \, \langle kl| \, . \tag{4}$$

η_i are the natural orbital occupation numbers, and Γ_{ijkl} are the second order density matrices expressed in terms of the NOs. At the Hartree-Fock level of theory the η_i equal 2 or 0 for a restricted closed shell calculation. In Density Functional Theory (DFT) no density matrix is defined although we pragmatically use the same expressions as at the Hartree-Fock level, but with Kohn-Sham orbitals, as experience has shown that this also gives chemically useful results [73]. At both these levels of theory, the second order reduced density matrix can be easily expressed in terms of the first order reduced density matrix (1RDM) which will help deriving bond indices. Atoms in Molecules (AIMs) can be obtained in many different ways from Eq. 3. Most generally, for the atomic electronic population on atom A, denoted N_A, one takes the expectation value of an operator $\hat{P}_A$

$$N_A = \left\{ \hat{P}_A \right\} = \mathrm{Tr}(\hat{P}_A \hat{\gamma}). \tag{5}$$

One can think of this equation loosely as "projecting" out an atom A from a density operator. The reason why many different AIMs exist is that different authors introduced different forms of $\hat{P}_A$, e.g.

1. Mulliken [74, 75]:

$$\hat{P}_A = \sum_{\sigma \in A} \sum_{\lambda} \left(|\sigma\rangle \left(\mathbf{S}^{-1} \right)_{\sigma\lambda} \langle \lambda| \right) \tag{6}$$

   where $\mathbf{S}^{-1}$ is the inverse overlap matrix and Greek letters signify non-orthogonal (often Gaussian) basis functions.

2. Roby [76]:

$$\hat{P}_A = \sum_{i_A \in A} |i_A\rangle \langle i_A| \tag{7}$$

where the functions $|i_A\rangle$ are occupied natural orbitals for atom A, i.e. those eigenstates obtained from a spherically averaged unrestricted Hartree-Fock or DFT calculation on atom A with eigenvalue η_i^A greater than 0.05.

Note the difference in these two Hilbert space operators for the atom A. For the Mulliken case, one summation is over all nonorthogonal basis functions centered on a specific atom and the second summation over all basis functions. The Mulliken formulation is not applicable for basis functions which do not have a natural center such as plane wave basis functions. Also, the summation over λ is over the entire basis set, which may become arbitrarily large. The Roby operator on the other hand always makes use of a limited number of orthogonal atomic functions. Both the Mulliken operator (Eq. 6) and the Roby projection operator (Eq. 7) are projection operators in the mathematical sense, i.e. that $\hat{P}_A$ is idempotent, $\hat{P}_A^2 = \hat{P}_A$. Note however, that whereas the sum of the atomic populations N_A equals the number of electrons N in the Mulliken case, this electron population conservation does not hold true of the Roby populations.

Besides these Hilbert-space methods, one also has real space methods whose population operators can be written in the form

$$\hat{P}_A = \int d\mathbf{r}\, |\mathbf{r}\rangle\, w_A(\mathbf{r})\, \langle \mathbf{r}|\,. \tag{8}$$

Substituting the population operator from Eq. 8 in Eq. 5 gives

$$N_A = \sum_i \eta_i \int d\mathbf{r}\, \langle i|\mathbf{r}\rangle\, w_A(\mathbf{r})\, \langle \mathbf{r}|i\rangle \tag{9}$$

where, for example, $\langle i|\mathbf{r}\rangle = \psi_i^*(\mathbf{r})$. Different methods that work directly in coordinate space exist. In the present paper both the QTAIM method [45, 77] is used where $w_A(\mathbf{r})$ is binary, i.e. either 1 or 0, and the Hirshfeld-I method [57, 78, 79] that uses a model of overlapping AIM and hence has $0 \leq w_A(\mathbf{r}) \leq 1$. In both cases real space is exhaustively partitioned, i.e. $\forall \mathbf{r} : \sum_A w_A(\mathbf{r}) = 1$ and

electron population is conserved.

Turning to bonding indices, we use two types of methods in the present study. These can be distinguished by the type of density matrices used. The first type relies on the 1RDM only, and uses the Roby populations [54,76]. First a two-atom (mathematical) projection operator for atoms A and B is introduced as

$$\hat{P}_{AB} = \sum_{k\in(A,B)} \sum_{l\in(A,B)} |k\rangle \left(\mathbf{S}_{AB}^{-1}\right)_{kl} \langle l| \tag{10}$$

where $\mathbf{S}_{AB}^{-1}$ is the inverse of the overlap matrix formed from the occupied natural orbitals on atoms A and B. Then the Roby-Gould bond index is defined as [54]

$$\tau_{AB} = \sqrt{c_{AB}^2 + i_{AB}^2}, \quad \text{where} \tag{11}$$

$$c_{AB} = \left\{ \frac{\hat{P}_A + \hat{P}_B - \hat{P}_{AB}}{2|\hat{P}_A + \hat{P}_B - \hat{P}_{AB}|} \right\}, \quad \text{and} \tag{12}$$

$$i_{AB} = \left\{ \frac{\hat{P}_A - \hat{P}_B}{2|\hat{P}_A - \hat{P}_B|} \right\} \tag{13}$$

are the covalent and ionic bond indices. The Roby-Gould bond index is best thought of as a two-dimensional quantity. The above equations involve functions of operators; such operator functions are fully characterized as having the same eigenstates as the original operator, except with eigenvalues which are the same function of the original operators' eigenvalues. In the present case, zero and unit eigenvalues are ignored in all equations as they would lead to infinities in one or the other denominator. As explained more fully elsewhere [54,80], these formulae arise naturally from the algebra of projection operators, and they generalise the notion of a chemical bond order as "the number of electrons in bonding orbitals minus the number of electrons in antibonding orbitals, divided by two". In practice, for simple organic or ionic compounds, they produce numerical results which are very compatible with those obtained by drawing standard Lewis structures. [54,80]

In contrast, Wiberg, Giambiagi, Mayer, Bader and co-workers [52, 81–84] introduced several indices that can all be gathered under the same umbrella [85] in the sense that they are integrals

over diatomic condensed exchange-correlation density matrices (XCD). The XCD is defined as

$$\rho^{\mathrm{xcd}}(\mathbf{r}_1,\mathbf{r}_1^{'};\mathbf{r}_2,\mathbf{r}_2^{'}) = \rho(\mathbf{r}_1,\mathbf{r}_1^{'})\rho(\mathbf{r}_2,\mathbf{r}_2^{'}) - 2\sum_{ijkl}\Gamma_{ijkl}\psi_i^*(\mathbf{r}_1)\psi_k(\mathbf{r}_1^{'})\psi_j^*(\mathbf{r}_2)\psi_l(\mathbf{r}_2^{'}). \tag{14}$$

All these bond indices can be called shared electron density indices (SEDI) [53] and essentially come down to different ways of projecting out the two atoms. In the present work only position-space operators are considered, notably the QTAIM operator and the Hirshfeld-I operator. At the closed shell single determinant level of theory (Hartree-Fock and pragmatically also Kohn-Sham DFT), the bond indices are given as:

$$\delta_{AB} = 4\sum_{i,j}^{N/2}\langle i|w_A|j\rangle\langle j|w_B|i\rangle \tag{15}$$

where the QTAIM and Hirshfeld-I data differ due to the difference in w_A.

Acknowledgement

Simon Grabowsky thanks the German Research Foundation (Deutsche Forschungsgemeinschaft, DFG) for funding within the Emmy Noether project GR 4451/1-1. The authors also thank Professor E. D. Jemmis (Indian Institute of Science, Bangalore, India) for providing access to a cluster used for computation of natural bond orbitals.

Supporting paragraph

The Supporting Information contains computational details, precise values of all plotted properties, ELI plots of the n-membered ring systems, an NBO analysis of the disiloxane-water complexes, and coordinates of the optimized geometries.

Conflicts of interest

The authors declare no conflicts of interest.

References

[1] G. V. Gibbs, R. T. Downs, D. F. Cox, N. L. Ross, C. T. Prewitt, K. M. Rosso, T. Lippmann, A. Kirfel, *Z. Kristallog.* **2008**, *223*(01-02), 01–40.

[2] G. V. Gibbs, A. F. Wallace, D. F. Cox, R. T. Downs, N. L. Ross, K. M. Rosso, *Am. Mineral.* **2009**, *94*(8-9), 1085–1102.

[3] R. K. Iler, *The chemistry of silica: solubility, polimerization, colloid and surface properties, and biochemistry*, Wiley Interscience, **1979**.

[4] R. West, L. S. Wilson, D. L. Powell, *J. Organomet. Chem.* **1979**, *178*(1), 5–9.

[5] V. Shklover, H.-B. Bürgi, A. Raselli, T. Armbruster, W. Hummel, *Acta Cryst. B* **1991**, *47*(4), 544–548.

[6] I. L. Karle, J. M. Karle, C. J. Nielsen, *Acta Cryst. C* **1986**, *42*(1), 64–67.

[7] J. Tossell, G. V. Gibbs, *Acta Cryst. A* **1978**, *34*(3), 463–472.

[8] J. E. Mark, *Acc. Chem. Res.* **2004**, *37*(12), 946–953.

[9] S. Grabowsky, M. F. Hesse, C. Paulmann, P. Luger, J. Beckmann, *Inorg. Chem.* **2009**, *48*(10), 4384–4393.

[10] S. Grabowsky, J. Beckmann, P. Luger, *Aust. J. Chem.* **2012**, *65*(7), 785–795.

[11] F. Weinhold, R. West, *Organometallics* **2011**, *30*(21), 5815–5824.

[12] F. Weinhold, R. West, *J. Am. Chem. Soc.* **2013**, *135*(15), 5762–5767.

[13] J. B. Nicholas, R. E. Winans, R. J. Harrison, L. E. Iton, L. A. Curtiss, A. J. Hopfinger, *J. Phys. Chem.* **1992**, *96*(20), 7958–7965.

[14] C. Eaborn, P. B. Hitchcock, P. Lickiss, *J. Organomet. Chem* **1984**, *264*, 119.

[15] A. I. Gusev, A. G. Los, Y. M. Varazhkin, M. M. Morgunova, D. Y. Zhinkin, *J. Struct. Chem* **1976**, *17*, 329.

[16] A. Spielberger, P. Gspaltl, H. Siegl, E. Hengge, K. Gruber, *J. Organomet. Chem.* **1995**, *499*(1), 241–246.

[17] C. Clobes, P. Jerabek, I. Nußbruch, G. Frenking, C. von Hänisch, *Eur. J. Inorg. Chem.* **2015**, (20), 3264–3273.

[18] C. von Hänisch, O. Hampe, F. Weigend, S. Stahl, *Angew. Chem. Int. Ed.* **2007**, *46*(25), 4775–4779.

[19] T. S. Cameron, A. Decken, I. Krossing, J. Passmore, J. M. Rautiainen, X. Wang, X. Zeng, *Inorg. Chem.* **2013**, *52*(6), 3113–3126.

[20] Y. Yokouchi, S. Ishida, T. Onodera, H. Oikawa, T. Iwamoto, *Chem. Commun.* **2018**, *54*(3), 268–270.

[21] K. Reuter, G. Thiele, T. Hafner, F. Uhlig, C. von Hänisch, *Chem. Commun.* **2016**, *52*(90), 13265–13268.

[22] F. Dankert, K. Reuter, C. Donsbach, C. von Hänisch, *Inorganics* **2018**, *6*(1), 15.

[23] F. Dankert, C. Donsbach, C.-N. Mais, K. Reuter, C. von Hänisch, *Inorg. Chem.* **2018**, *57*(1), 351–359.

[24] R. West, L. S. Whatley, K. J. Lake, *J. Am. Chem. Soc.* **1961**, *83*(4), 761–764.

[25] G. V. Gibbs, *Am. Mineral.* **1982**, *67*(5-6), 421–450.

[26] J. Passmore, J. M. Rautiainen, *Eur. J. Inorg. Chem.* **2012**, (36), 6002–6010.

[27] A. Vegas, R. Notario, E. Chamorro, P. Pérez, J. F. Liebman, *Acta Cryst. B* **2013**, *69*(2), 163–175.

[28] C. Martín-Fernández, M. M. Montero-Campillo, I. Alkorta, J. Elguero, *J. Phys. Chem. A* **2017**, *121*(39), 7424–7431.

[29] C. Martín-Fernández, M. M. Montero-Campillo, I. Alkorta, J. Elguero, *Mol. Phys.* **2018**, *116*(12), 1539–1550.

[30] I.-T. Moraru, P. M. Petrar, G. Nemes, *J. Phys. Chem. A* **2017**, *121*(12), 2515–2522.

[31] G. V. Gibbs, K. M. Rosso, D. M. Teter, M. B. Boisen Jr, M. S. T. Bukowinski, *J. Mol. Struct.* **1999**, *485*, 13–25.

[32] R. J. Gillespie, S. A. Johnson, *Inorg. Chem.* **1997**, *36*(14), 3031–3039.

[33] V. G. Tsirelson, O. A. Evdokimova, E. L. Belokoneva, V. S. Urusov, *Phys. Chem. Miner.* **1990**, *17*(3), 275–292.

[34] G. V. Gibbs, J. W. Downs, M. B. Boisen, *Rev. Mineral. Geochem.* **1994**, *29*(1), 331–368.

[35] A. Almenningen, O. Bastiansen, V. Ewing, K. Hedberg, M. Traetteberg, *Acta Chem. Scand.* **1963**, *17*(9), 2455–2460.

[36] M. J. Barrow, E. A. V. Ebsworth, M. M. Harding, *Acta Cryst. B* **1979**, *35*(9), 2093–2099.

[37] F. Stone, D. Seyferth, *J. Inorg. Nucl. Chem.* **1955**, *1*(1-2), 112–118.

[38] H. Oberhammer, J. E. Boggs, *J. Am. Chem. Soc.* **1980**, *102*(24), 7241–7244.

[39] F. Weinhold, C. R. Landis, *Valency and bonding: a natural bond orbital donor-acceptor perspective*, Cambridge University Press, **2005**.

[40] J. M. L. Martin, G. de Oliveira, *J. Chem. Phys.* **1999**, *111*(5), 1843–1856.

[41] G. Frenking, S. Shaik, *The chemical bond: fundamental aspects of chemical bonding*, John Wiley & Sons, **2014**.

[42] C. Gatti, *Z. Kristallog.* **2005**, *220*(5/6), 399–457.

[43] J. Henn, D. Leusser, D. Stalke, *J. Comput. Chem.* **2007**, *28*(14), 2317–2324.

[44] M. Fugel, J. Beckmann, D. Jayatilaka, G. V. Gibbs, S. Grabowsky, *Chem. Eur. J.* **2018**, *24*, 6248–6261.

[45] R. Bader, *Atoms in Molecules, A Quantum Theory*, Oxford Science Publications, **1990**.

[46] M. Kohout, *Int. J. Quantum Chem.* **2004**, *97*(1), 651–658.

[47] C. Gatti, F. Cargnoni, L. Bertini, *J. Comput. Chem.* **2003**, *24*(4), 422–436.

[48] E. Glendening, C. Landis, F. Weinhold, *WIREs Comput. Mol. Sci.* **2012**, *2*, 1–42.

[49] E. D. Glendening, F. Weinhold, *J. Comput. Chem.* **1998**, *19*(6), 593–609.

[50] E. D. Glendening, F. Weinhold, *J. Comput. Chem.* **1998**, *19*(6), 610–627.

[51] E. D. Glendening, J. Badenhoop, F. Weinhold, *J. Comput. Chem.* **1998**, *19*(6), 628–646.

[52] X. Fradera, M. A. Austen, R. F. W. Bader, *J. Phys. Chem. A* **1999**, *103*(2), 304–314.

[53] R. Ponec, D. L. Cooper, *J. Mol. Struct.* **2005**, *727*(1-3), 133–138.

[54] M. D. Gould, C. Taylor, S. K. Wolff, G. S. Chandler, D. Jayatilaka, *Theor. Chem. Acc.* **2008**, *119*(1-3), 275–290.

[55] J. Beckmann, S. Grabowsky, *J. Phys. Chem. A* **2007**, *111*(10), 2011–2019.

[56] R. McWeeny, *Coulson's valence*, Oxford University Press, USA, **1979**.

[57] P. Bultinck, P. W. Ayers, S. Fias, K. Tiels, C. Van Alsenoy, *Chem. Phys. Lett.* **2007**, *444*(1-3), 205–208.

[58] K. B. Wiberg, P. R. Rablen, *J. Comput. Chem.* **1993**, *14*(12), 1504–1518.

[59] P. J. Stephens, F. J. Devlin, C. F. Chabalowski, M. J. Frisch, *J. Phys. Chem.* **1994**, *98*, 11623.

[60] S. Grimme, S. Ehrlich, L. Goerigk, *J. Comput. Chem.* **2011**, *32*(7), 1456–1465.

[61] M. J. Frisch, G. W. Trucks, H. B. Schlegel, G. E. Scuseria, M. A. Robb, J. R. Cheeseman, G. Scalmani, V. Barone, G. A. Petersson, H. Nakatsuji, X. Li, M. Caricato, A. V. Marenich, J. Bloino, B. G. Janesko, R. Gomperts, B. Mennucci, H. P. Hratchian, J. V. Ortiz, A. F. Izmaylov, J. L. Sonnenberg, D. Williams-Young, F. Ding, F. Lipparini, F. Egidi, J. Goings, B. Peng, A. Petrone, T. Henderson, D. Ranasinghe, V. G. Zakrzewski, J. Gao, N. Rega, G. Zheng, W. Liang, M. Hada, M. Ehara, K. Toyota, R. Fukuda, J. Hasegawa, M. Ishida, T. Nakajima, Y. Honda, O. Kitao, H. Nakai, T. Vreven, K. Throssell, J. A. Montgomery, Jr., J. E. Peralta, F. Ogliaro, M. J. Bearpark, J. J. Heyd, E. N. Brothers, K. N. Kudin, V. N. Staroverov, T. A. Keith, R. Kobayashi, J. Normand, K. Raghavachari, A. P. Rendell, J. C. Burant, S. S. Iyengar, J. Tomasi, M. Cossi, J. M. Millam, M. Klene, C. Adamo, R. Cammi, J. W. Ochterski, R. L. Martin, K. Morokuma, O. Farkas, J. B. Foresman, D. J. Fox, Gaussian 09, revision D. 01, **2009**.

[62] E. D. Glendening, C. R. Landis, F. Weinhold, *J. Comput. Chem.* **2013**, *34*(16), 1429–1437.

[63] T. A. Keith, AIMAll, version 13.05. 06, TK Gristmill Software, Overland Park KS, USA, **2013**.

[64] M. Kohout, DGrid, version 4.6, Dresden, Germany, **2011**.

[65] C. B. Hübschle, P. Luger, *J. Appl. Crystallogr.* **2006**, *39*(6), 901–904.

[66] D. Jayatilaka, D. J. Grimwood, in *International Conference on Computational Science*, Springer, 142–151.

[67] H.-J. Werner, P. J. Knowles, G. Knizia, F. R. Manby, M. Schütz, *Wiley Interdiscip. Rev.-Comput. Mol. Sci.* **2012**, *2*(2), 242–253.

[68] A. Karton, J. M. L. Martin, *J. Chem. Phys.* **2012**, *136*(12), 124114.

[69] K. A. Peterson, D. Feller, D. A. Dixon, *Theor. Chem. Acc.* **2012**, *131*(1), 1079.

[70] T. Helgaker, W. Klopper, D. P. Tew, *Mol. Phys.* **2008**, *106*(16-18), 2107–2143.

[71] P. Bultinck, P. Popelier, *Atoms in Molecules and Population Analysis*, Taylor and Francis, **2009**, 215–227.

[72] R. G. Parr, P. W. Ayers, R. F. Nalewajski, *J. Phys. Chem. A* **2005**, *109*(17), 3957–3959.

[73] J. Poater, M. Duran, M. Sola, B. Silvi, *Chem. Rev.* **2005**, *105*(10), 3911–3947.

[74] R. S. Mulliken, *J. Chem. Phys.* **1955**, *23*(10), 1833–1840.

[75] R. S. Mulliken, *J. Chem. Phys.* **1955**, *23*(10), 1841–1846.

[76] K. R. Roby, *Mol. Phys.* **1974**, *27*(1), 81–104.

[77] R. F. W. Bader, *Chemical Reviews* **1991**, *91*(5), 893–928.

[78] P. Bultinck, C. Van Alsenoy, P. W. Ayers, R. Carbo-Dorca, *J. Chem. Phys.* **2007**, *126*(14), 144111.

[79] P. Bultinck, D. L. Cooper, D. Van Neck, *Phys. Chem. Chem. Phys.* **2009**, *11*(18), 3424–3429.

[80] K. Alhameedi, B. Bohman, A. Karton, D. Jayatilaka, *Int. J. Quantum Chem.* **2018**, e25603.

[81] K. Wiberg, *Tetrahedron* **1968**, *24*(3), 1083–1096.

[82] M. Giambiagi, M. Giambiagi, D. R. Grempel, C. D. Heymann, *J. Chim. Phys.* **1975**, *72*(1), 15–22.

[83] R. F. W. Bader, M. E. Stephens, *Chem. Phys. Lett.* **1974**, *26*(3), 445–449.

[84] R. F. W. Bader, A. Streitwieser, A. Neuhaus, K. E. Laidig, P. Speers, *J. Am. Chem. Soc.* **1996**, *118*(21), 4959–4965.

[85] P. Bultinck, D. L. Cooper, R. Ponec, *J. Phys. Chem. A* **2010**, *114*(33), 8754–8763.